Changes in substrate availability in *Escherichia coli* lead to rapid metabolite, flux and growth rate responses

Hilal Taymaz-Nikerel [a,*], Marjan De Mey [b], Gino Baart [c], Jo Maertens [b], Joseph J. Heijnen [a], Walter van Gulik [a]

[a] Department of Biotechnology, Delft University of Technology, Kluyver Centre for Genomics of Industrial Fermentation, Julianalaan 67, 2628 BC Delft, The Netherlands
[b] Department of Biochemical and Microbial Technology, Centre of Expertise-Industrial Biotechnology and Biocatalysis, Ghent University, Coupure Links 653, 9000 Ghent, Belgium
[c] Department of Applied Mathematics, Biometrics and Process Control, Ghent University, Coupure Links 653, 9000 Ghent, Belgium

ARTICLE INFO

ABSTRACT

The interactions between the intracellular metabolome, fluxome and growth rate of *Escherichia coli* after sudden glycolytic/gluconeogenic substrate shifts are studied based on pulses of different substrates to an aerobic glucose-limited steady-state (dilution rate=0.1 h^{-1}). After each added glycolytic (glucose) and gluconeogenic (pyruvate and succinate) substrate pulse, no by-products were secreted and a pseudo steady state in flux and metabolites was achieved in about 30–40 s. In the pulse experiments a large oxygen uptake capacity of the cells was observed. The *in vivo* dynamic responses showed massive reorganization and flexibility (1/100–14-fold change) of extra/intracellular metabolic fluxes, matching with large changes in the concentrations of intracellular metabolites, including reversal of reaction rate for pseudo/near equilibrium reactions. The coupling of metabolome and fluxome could be described by Q-linear kinetics. Remarkably, the three different substrate pulses resulted in a very similar increase in growth rate (0.13–0.3 h^{-1}). Data analysis showed that there must exist as yet unknown mechanisms which couple the protein synthesis rate to changes in central metabolites.

© 2013 Elsevier Inc. All rights reserved.

1. Introduction

There has been considerable effort to unravel the structure and function of metabolic networks (Fiehn, 2001; Kim et al., 2010; Liao, 1993), and there has been a consensus that systems biology approaches are necessary to understand the complex interactions involved within and among the transcriptome, proteome, metabolome and fluxome of a living system. Systems biology aims at gaining quantitative insight into the mechanisms in (subsystems of) living cells through combining mathematical models with experimental evidence (Heinemann and Sauer, 2010). Improvement of microorganisms towards a higher product rate/yield is generally expected to benefit from genome scale kinetic models in which all major metabolic fluxes can be calculated as a function of enzyme levels and enzyme kinetic properties. Such a model would qallow the identification of premium gene targets for metabolic qpathway engineering, thus avoiding labor intensive trial-and-error genetic engineering and strain testing (Nielsen, 2001; Stephanopoulos, 1994).

In vivo kinetic modeling of metabolism requires experimental information on metabolic fluxes, enzyme levels and concentrations of metabolites under a number of different conditions, which can be obtained from perturbations of controlled steady-state cultures (Nikerel et al., 2006; Oldiges and Takors, 2005; Theobald et al., 1997; Visser et al., 2002). If perturbation experiments are carried out in a sufficiently short time frame (minutes), the enzyme levels can be assumed constant and only measurements of concentrations of extra- and intracellular metabolites are required for kinetic modeling purposes (Chassagnole et al., 2002). The measured extracellular concentration profiles allow mass-balance-based calculation of the associated uptake/secretion rates from which, via metabolic flux analysis, all reaction fluxes in the metabolic network can be obtained (Taymaz-Nikerel et al., 2011). The combination of changed fluxes and changed intracellular metabolite concentrations provides the required information to deduce the *in vivo* kinetic properties of the enzymes.

For *Escherichia coli* it was recently demonstrated that such rapid perturbation experiments can be performed in the BioScope (De Mey et al., 2010), a mini plug-flow reactor which can be coupled to *e.g.* a steady state chemostat. This device allows carrying out stimulus response experiments within a short time interval (seconds to minutes) whereby samples can be taken with

intervals of sub seconds to seconds. From pulse response experiments with *E. coli* it was found that the induced changes in metabolite levels occur indeed very fast (< 1 s) (Chassagnole et al., 2002; De Mey et al., 2010; Schaefer et al., 1999), requiring pulse experiments within a time frame of 20–40 s. Although with such tools *in vivo* data can be acquired, the information content is generally limited because of the complexity of the rate equations, the resulting large number of parameters to be estimated (Nikerel et al., 2009), and the correlation between metabolite and flux data (Canelas et al., 2011). As an efficient solution to this problem, Canelas et al. (2011) introduced a new simplified kinetic format, named "Q-linear kinetics", based on classifying reactions according to their thermodynamic state. The classification was based on the relation between the reaction quotient Q and the flux of a reaction, which at the same time allows determining the *in vivo* K_{eq} of that reaction.

Recently we presented a method to resolve the rapid (seconds time scale) dynamics of the growth rate of *E. coli* in a pulse experiment (Taymaz-Nikerel et al., 2011). When *E. coli* cells cultured in a glucose-limited chemostat at $D = 0.1 \ h^{-1}$ ($C_S \sim 10$ mg/L) were suddenly exposed to glucose excess ($C_S \sim 500$ mg/L), a 3–4-fold increase in the growth rate and all other network fluxes was observed within 40–60 s. This observation, which was supported by independent measurements of intracellular metabolites/turnover times, implies a 3–4-fold increase (due to the 3–4-fold increase in growth rate) in the rate of protein synthesis by the ribosomes within tens of seconds, which is very remarkable. This significant increase in the growth rate should be taken into consideration in the parametrization of dynamic models using pulse response data. However, even in the most comprehensive dynamic model of *E. coli* published, the specific growth rate is assumed to remain constant at the steady-state value during the glucose pulse (Chassagnole et al., 2002).

In this study, we obtained further evidence for this rapid growth rate response by carrying out pulse experiments, with glucose and two gluconeogenic substrates (*i.e.*, pyruvate and succinate).

2. Materials and methods

2.1. Strain, medium and chemostat conditions

The *E. coli* K12 MG1655 [λ^-, F$^-$, rph^{-1}] strain was cultivated (temperature 37 °C, pH 7) in aerobic glucose-limited chemostat cultures with minimal medium at a dilution rate (D) of 0.1 h^{-1} in 7 L laboratory bioreactors with a working mass of 4 kg, controlled by weight (Applikon, Schiedam, The Netherlands). The preculture conditions, medium composition, chemostat conditions (temperature control, pH control, overpressure, aeration rate, stirrer speed, dissolved oxygen and off-gas measurements) were as described by De Mey et al. (2010). It is noteworthy that the here used nutrient medium was designed with much lower Cl$^-$ and K$^+$ concentrations compared to the medium used by Taymaz-Nikerel et al. (2011) and Taymaz-Nikerel et al., 2009, because too high Cl$^-$ concentrations were found to interfere with the liquid chromatography (LC) part of the LC-mass spectrometry (MS) analysis of intracellular metabolites.

2.2. Experimental design

The advantage of the information richness of the data obtained from the rapid BioScope pulse experiments comes with a disadvantage: the change in the extracellular concentration of the pulsed substrate cannot be quantified accurately in the short time period of the pulse experiment due to its small change, leading to

difficulties in the quantification of the uptake rate of the substrate. For this purpose, samples should be taken during a longer period of time, which cannot be achieved in the BioScope but which is possible in a bioreactor (Taymaz-Nikerel et al., 2011). More importantly, applying pulses in a bioreactor also permits monitoring the changes in the off-gas O_2/CO_2 and dissolved O_2 concentrations, thus allowing the time (on a seconds time scale) resolved quantification of the O_2 uptake rate (Taymaz-Nikerel et al., 2011; Wu et al., 2006). O_2 and substrate uptake rates are essential to construct carbon and redox balances (Nasution, 2007; Wu et al., 2006), allowing the quantification of changes in growth rate on a seconds time scale, which is needed to calculate the *in vivo* metabolic fluxes during the rapid pulse experiment. Therefore, rapid pulse experiments were realized both in the bioreactor (to obtain the fluxes) and in the BioScope (to obtain the metabolite levels) (see below).

2.3. Rapid substrate pulse experiments

Short-term rapid pulse experiments in the bioreactor and in the BioScope were carried out as described previously (De Mey et al., 2010; Taymaz-Nikerel et al., 2011). To prevent oxygen limitation during the pulse experiments, the aeration gas of the bioreactor (1.67 L/min normal air) was blended with 0.5 L/min 100% O_2, which increased the volumetric concentration to about 39% O_2. Oxygen blending was started at least one hour before each pulse experiment. Pulses to the bioreactor were performed with 20 mL pulse solution, directly injected in the bioreactor by means of a sterile syringe. The feed pump and broth outflow were stopped at the start of a pulse experiment and restarted at 510 s after each pulse.

For all pulses carried out in the Bioscope, the gas channel of the BioScope was continuously flushed with enriched air (63% O_2) to prevent oxygen limitation. Pulses in the BioScope were carried out at two different flow rates (at 1.8 mL/min broth + 0.2 mL/min pulse and 3.6 mL/min broth + 0.4 mL/min pulse) to cover two time frames (8 and 40 s), as described by De Mey et al. (2010).

All perturbations were designed such that the initial carbon concentration after each substrate pulse would be 16.7 mCmol/L (equivalent to 0.5 g/L glucose). The pulse solutions used in the BioScope were therefore 27.8 mM glucose, 55.5 mM pyruvate and 41.6 mM succinate. In that case the initial bulk concentrations directly after the addition of the pulse were either 2.78 mM glucose, 5.55 mM pyruvate or 4.16 mM succinate, both in the bioreactor and BioScope experiments.

2.4. Rapid sampling for extra-/intracellular metabolites

The differential method (Taymaz-Nikerel et al., 2009) was applied to obtain the amounts of intracellular metabolites collected during the steady-state as well as during the transient states for both the bioreactor and the BioScope. The required broth and filtrate sampling was carried out as described by Taymaz-Nikerel et al. (2009). The steady-state preceding each pulse was sampled twice and each sample was analyzed in duplicate. For intracellular metabolite determination during the pulse experiment, only sampling of broth was performed (De Mey et al., 2010; Taymaz-Nikerel et al., 2011) at each time point and analyzed in duplicate.

For measurements of glucose and possible secreted by-products (organic acids and alcohols) fast filtration sampling using cold stainless steel beads was applied (both for the bioreactor and the BioScope), as described previously (De Mey et al., 2010; Taymaz-Nikerel et al., 2011).

2.5. Extraction of metabolites

Metabolites were extracted in 75% boiling ethanol (3 min, 90 °C) as described in Taymaz-Nikerel et al. (2009). Before extraction, 100 μL of 100% U-^{13}C-labeled cell extract was added to every sample as internal standard for isotope dilution mass spectrometry (IDMS)-based metabolite quantification (Wu et al., 2005). The preparation of the 100% U-^{13}C-labeled yeast cell extract can be found in Wu et al. (2005).

2.6. Analytical techniques

Measurement of cell dry weight, residual glucose, total organic carbon and intracellular metabolite concentrations (glycolysis, TCA cycle, PPP, adenine nucleotides and free amino acids) were carried out as described previously (De Mey et al., 2010; Taymaz-Nikerel et al., 2009). The filtrate samples for extracellular pyruvate determination during the pyruvate pulse were kept in the fridge (about 4 °C) about a few days until analysis (see Supplementary Information Section 8). Pyruvate concentration was measured with HPLC (Aminex HPX-87H ion exclusion column, Bio-Rad, CA, USA) with a refractive index detector (Waters 2414) and UV detector at 210 nm. The column was eluted with phosphoric acid (15 mM) at a column temperature of 59 °C and a flow rate of 0.6 mL/min. The extracellular succinate concentration during the succinate pulse was quantified enzymatically (Boehringer Mannheim/R-Biopharm, Roche).

The supernatant samples obtained after the pulses were extensively analyzed for the presence of possible by-products. HPLC (Aminex HPX-87H ion exclusion column, Bio-Rad, CA, USA; the column was eluted with 1.5 mM phosphoric acid except for pyruvate quantification) and LC-MS/MS (van Dam et al., 2002) analysis were performed to check the presence of ethanol, acetaldehyde, glyoxylate, acetate, formate, lactate, fumarate, pyruvate, oxaloacetate, malate, succinate, citrate and α-ketoglutarate.

2.7. Biomass-specific uptake and production rates

The mass-balance-based and reconciled biomass-specific rates (glucose consumption ($-q_S$), oxygen consumption ($-q_{O_2}$), carbon dioxide production (q_{CO_2}), growth (μ) and cell lysis (q_{lysis})) during steady-state were calculated as described before (De Mey et al., 2010; Taymaz-Nikerel et al., 2009).

$-q_S$ and $-q_{O_2}$ during the pulses were obtained from experimental data as described by Taymaz-Nikerel et al. (2011). To obtain the dynamic $-q_{O_2}(t)$, the dynamic DO mass balance was applied using the measured DO-profile during the pulse, a validated k_La value and the properly validated measurement of dynamic response of the DO probe (see Supplementary Information Section 2). $\mu(t)$ was then calculated as follows: In pseudo-steady-state at $t > 30$–40 s, μ follows from the degree of reduction balance, $\gamma_S(-q_S) = \gamma_X\mu + \gamma_{O_2}(-q_{O_2})$, where any possible secreted product was absent, ($\gamma_S = 24$ for glucose, 10 for pyruvate and 14 for succinate, $\gamma_X = 4.3$ (Taymaz-Nikerel et al., 2010), $\gamma_{O_2} = -4$) using the experimentally obtained $-q_{O_2}(t)$ and $-q_S(t)$. During the transient ($t < 30$–40 s), large changes in metabolite concentrations prevent the use of the simple γ-balance. The dynamic pattern of μ during the transient ($t < 30$–40 s) then follows from $-q_{O_2}(t)$ and the assumption that the yield of produced biomass on consumed O_2 ($\mu/-q_{O_2}$) is constant during the transient. Supplementary Information Section 3 shows that this was indeed true for the studied range of growth rates, 0.13–0.3 h^{-1}.

2.8. Intracellular metabolic fluxes and metabolite turnover times

The intracellular fluxes during the steady-state and transient state were calculated with metabolic flux analysis using the appropriate metabolic network of E. coli. This assumes, in the period before metabolite steady state (< 40 s), applicability of metabolite pseudo-steady-state, which holds due to the observed very short turnover time of glycolytic metabolites (< 3 s).

The applied metabolic network model for growth on glucose, containing 276 biochemical reactions, was the one described by Taymaz-Nikerel et al. (2010). For the pyruvate and succinate networks, PEP-glyoxylate route (isocitrate lyase ICL, malate synthase MALS, PEP carboxykinase PPCK) was added and the phosphofructokinase (PFK) reaction was replaced with the fructose-bisphosphatase (FBP) reaction. Additionally PEP carboxylase and the oxidative PPP reactions were set to 0. These choices will be motivated in the appropriate results section. The turnover times of the intracellular pools were calculated as described by Taymaz-Nikerel et al. (2011).

2.9. Calculation of the reaction quotient Q, intracellular NAD$^+$/NADH ratio, energy charge

Thermodynamic feasibility of the direction of fluxes (see also Canelas et al. (2011)) was judged by calculating (using the measured intracellular concentrations of metabolites) reaction quotient Q of intracellular pseudo and near-equilibrium reactions. Q, NAD$^+$/NADH ratio and energy charge were calculated as described before (De Mey et al., 2010; Taymaz-Nikerel et al., 2009). For the NAD$^+$/NADH ratio calculation, the concentration of F6P (not successfully analyzed in the transient state) was calculated from G6P and the equilibrium constant of the reaction phosphoglucose isomerase (PGI) under the assumption of PGI equilibrium.

3. Results

3.1. Fluxes and concentrations of metabolites at steady-state

E. coli was grown under identical conditions in two independent aerobic glucose-limited chemostats (experiments 1 and 2) at a dilution rate of 0.1 h^{-1} on a defined mineral medium. The chemostats behaved very similar, as can be seen from the characteristics of the steady-state presented and discussed in Supplementary Information Section 1 (Supplementary Tables 1–4).

In experiment 1 (designed to obtain the fluxes during the pulse), the chemostat steady-state was perturbed in the bioreactor by switching off the glucose feed, immediately followed by injection of the pulse substrate. Three different substrate pulses (glucose, pyruvate and succinate) were given at intervals of 24 h in succession (~2.5 residence times in between the pulses). For each pulse, the amount of carbon injected was the same (16.7 mmol). At 8.5 min, after each substrate pulse, the glucose feed was switched on again, whereafter the system rapidly returned back to glucose-limited chemostat conditions. It was observed that after the injected substrates had been consumed, which occurred within about 5 min after each pulse, the glucose-limited steady-state fluxes were recovered rapidly. Intracellular metabolite levels were quantified at six time points (before and after each of the three substrate pulses given to the bioreactor). It was found that in addition to the fluxes, also the metabolite steady-state was completely recovered after each different substrate pulse (see Supplementary Table 3).

In experiment 2 (designed to obtain the short term dynamics of the intracellular metabolite concentrations during the pulse

experiment), the biomass present in the second chemostat was perturbed outside the bioreactor, using the BioScope mini bioreactor, with the same three substrates. The concentrations of metabolites during glucose-limited steady-state chemostat conditions were analyzed before and after the substrate pulses in the BioScope (Supplementary Table 3). Comparing experiments 1 and 2 (carried out after 49.8 and 50.3 h of chemostat cultivation, and representing about 7 residence times after the start of feeding) showed a good reproducibility of the steady-state levels of most metabolites, as was also observed by De Mey et al. (2010).

3.2. Extracellular fluxes at transient state

To be able to calculate the change in the growth rate, μ, as response to each substrate pulse, the specific substrate uptake rate, $-q_S$, oxygen consumption rate, $-q_{O_2}$, and secretion rate of by-product(s) during the substrate pulse are required (see Section 2 and Supplementary Information Sections 2 and 3). Quantification of $-q_{O_2}$ during the pulse experiments requires measurements of off-gas O_2/CO_2 and dissolved O_2 (DO), which cannot be realized in the BioScope. To obtain the dynamics of $-q_S$ and $-q_{O_2}$, the pulse experiments were repeated in the bioreactor, whereby on-line measurements were performed during a longer time period ($\sim$900 s) than the duration of the pulses in the BioScope (40 s).

The continuously monitored DO, pH (controlled at 7) and off-gas concentrations of O_2 and CO_2 during each substrate perturbation are shown in Supplementary Figs. 3–5, respectively. By using O_2-enriched air for aeration, O_2 limitation, which would occur as a result of the increased oxygen uptake rate of the culture during the pulse experiment was prevented. Due to the O_2 enrichment, this was prevented in all three pulse experiments, as can be seen from the dissolved oxygen profiles (Supplementary Figs. 3–5). An extensive analysis of the culture supernatant revealed that under these conditions no significant by-product formation occurred during any of the pulse experiments, which agrees with was found for the glucose pulse experiment by Taymaz-Nikerel et al. (2011).

The dynamics of the on-line measurements during the substrate excess phase of the pulse experiments (0–275 s for glucose, 0–200 s for pyruvate, and 0–220 s for succinate) (Supplementary Figs. 3–5) showed a steep decrease of the DO concentration and steeply decreased off-gas O_2 and increased off-gas CO_2 levels, clearly confirming a steep increase in O_2-consumption and CO_2 production due to the increased substrate consumption rate. For the glucose pulse one would expect that the amounts of consumed O_2 (represented by ΔO_2 in the gas phase) and produced CO_2 (represented by ΔCO_2 in the gas phase) would be equal when glucose is metabolized aerobically (respiratory quotient ≈ 1) and no by-product formation would occur. However, we observed that ΔCO_2 was always much lower than ΔO_2 (see Supplementary Figs. 3–5). The reason for this is that part of the produced CO_2 remains in the broth as HCO_3^-, leading to significant H^+ release. This was confirmed from the measured decrease in pH after the glucose pulse (Supplementary Fig. 3), and the absence of pH changes after the pyruvate pulse (Supplementary Fig. 4, for explanation see Section 5) and an increase of the pH after the succinate pulse (Supplementary Fig. 5, for explanation see Section 5). Between substrate depletion (275–510 s for glucose, 200–510 s for pyruvate, and 220–510 s for succinate) and restart of the chemostat feed, the expected opposite behavior of the on-line measurements was observed in all cases, where O_2 consumption and CO_2 production decreased rapidly and the pH increased (due to CO_2-stripping). This rapid starvation response clearly confirms the absence of significant amounts of secreted by-products, which otherwise would have served as alternative carbon sources after depletion of the pulsed substrate. After restart of chemostat

feeding and broth outflow (>510 s, leading to a constant glucose supply rate equal to the previous steady-state value) all on-line extracellular measurements returned to their previous steady-state values within 4 min.

Glucose pulse: Directly after injection, the glucose concentration was observed to decrease in a linear fashion and was depleted after 275 s (Fig. 1A). This decrease corresponded to a glucose uptake rate of 96.4 mmol CmolX^{-1} h^{-1} (Fig. 1B), which was 2.3-fold higher than the steady-state value (Supplementary Table 1). The oxygen uptake rate reached a pseudo-steady-state (pss) value of about 280 mmol CmolX^{-1} h^{-1} (also about 2.3-fold higher than the reference state) 40 s after the addition of the glucose, and remained at that value during the whole further glucose excess period, up to 275 s (Fig. 1C). The specific growth rate, μ, *vs*. time during the pseudo-steady-states which was reached after the pulse ($t > 30$–40 s) was calculated from the degree of reduction balance using the experimentally obtained $-q_{O_2}$ and $-q_S$. During the transient ($t < 30$–40 s), μ was calculated from the q_{O_2} profile and the assumption that the yield of produced biomass on consumed O_2 ($\mu/-q_{O_2}$) was constant during the transient (see Section 2). Fig. 1D shows that during glucose excess the calculated growth rate rapidly increased (within 40 s) to a pseudo steady state value of about 0.28 h^{-1} ($\sim$2.2-fold increase).

Pyruvate pulse: Also, the pulsed pyruvate was utilized immediately and showed a linear decrease in concentration. The pyruvate was depleted already after 200 s (Fig. 1E), much faster than glucose. The pyruvate uptake rate was calculated to be 255 mmol CmolX^{-1} h^{-1} (Fig. 1F) and appeared, with respect to carbon uptake, more than 30% higher than the glucose uptake rate.

In *E. coli*, pyruvate is transported by a specific active transport system that is an energy-dependent process (Lang et al., 1987). Although the exact mechanism is unknown, it is evident, from the immediate maximal pyruvate uptake, that the required transporters must have been present when the cells were cultivated under aerobic glucose-limited conditions.

As response to the pyruvate pulse the oxygen uptake rate nearly tripled, from a steady state value of 116 to 320 mmol CmolX^{-1} h^{-1}, already 40 s after the pulse (Fig. 1G). Also in this case it was found that the growth rate μ increased very rapidly (< 40 s), from a steady-state value of 0.13 h^{-1} to 0.29 h^{-1} (Fig. 1H), similar to the growth rate reached after glucose pulse.

Succinate pulse: The pattern of the extracellular succinate concentration after the pulse is shown in Fig. 1I. It was observed that extracellular succinate did not decrease linearly (as was observed for glucose and pyruvate). Instead, the uptake rate slowed down at decreasing succinate concentration, indicating a low affinity of the succinate uptake system. Succinate uptake could be described with hyperbolic uptake kinetics ($-q_S = -q_S^{max} C_S/K_S + C_S$) with $K_S = 0.20 \pm 0.03$ mM succinate and $-q_S^{max} = 259 \pm 29$ mmol succinate CmolX^{-1} h^{-1} (see Fig. 1J). Under aerobic conditions, C_4-dicarboxylates have been reported to be taken up by *E. coli* using the Dct system, that has an apparent K_M of 0.010–0.020 mM and is driven by the electrochemical proton gradient (Gutowski and Rosenberg, 1975). Our results reveal that a succinate uptake system with high capacity but a low affinity was present in our glucose-limited *E. coli* cells; with an estimated affinity constant, which is about 10 times higher than reported by Gutowski and Rosenberg (1975).

After the succinate pulse the oxygen uptake rate rapidly increased to a maximum value of 510 mmol CmolX^{-1} h^{-1} at 40 s after the pulse, which was 4.4-fold higher than during glucose limited steady-state chemostat growth (Fig. 1K). Thereafter, $-q_{O_2}$ decreased due to the hyperbolically decreasing succinate uptake rate. After the succinate pulse, the calculated growth rate
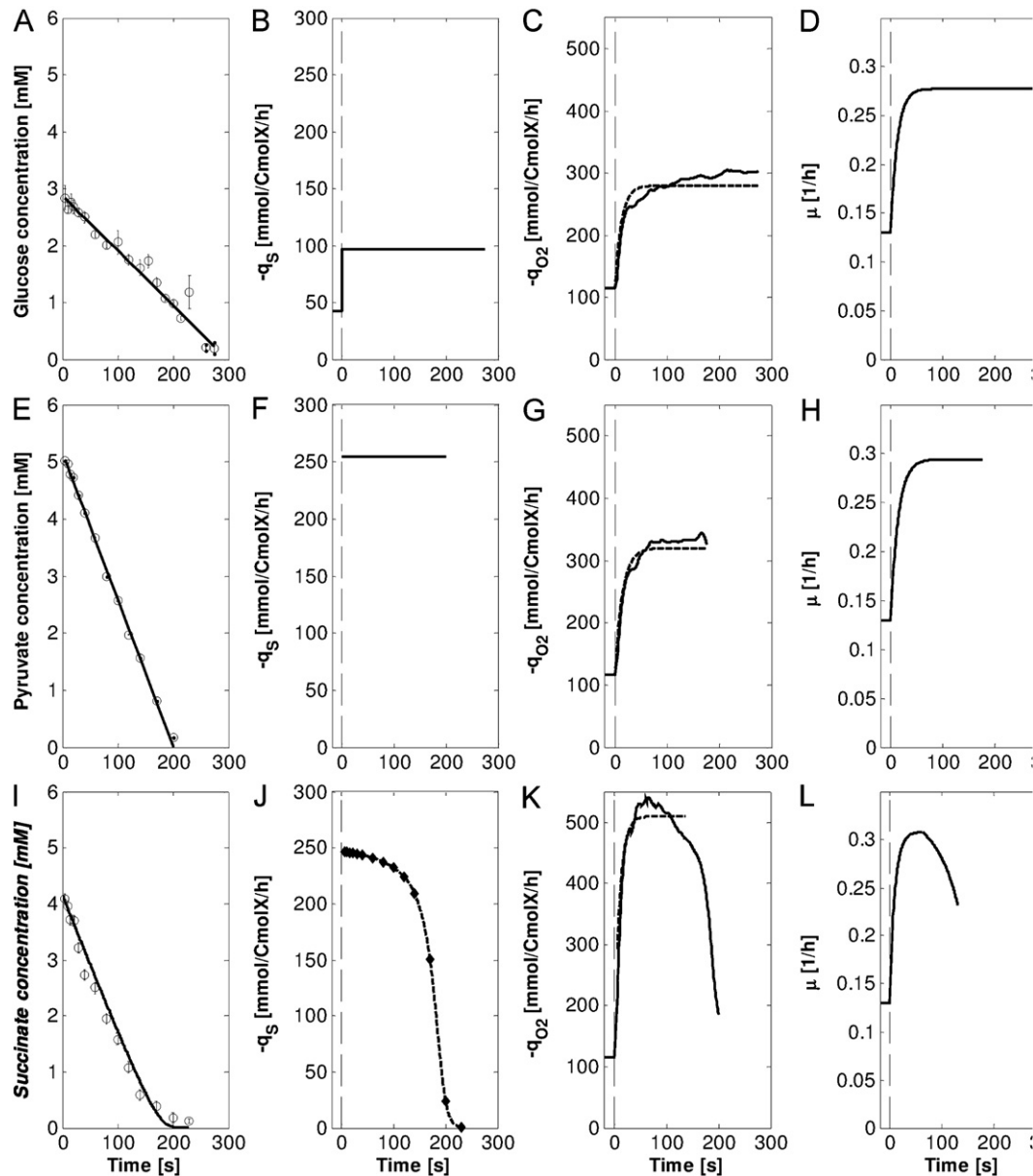
Fig. 1. Glucose (top row), pyruvate (middle row) and succinate (bottom row) pulses given in the bioreactor. (A, E, and I) Measured residual substrate concentration, (B, F, and J) mass balance-derived substrate uptake rate ($-q_S$), (C, G, and K) mass balance-derived oxygen uptake rate ($-q_{O_2}$), dashed line: estimated, and (D, H, and L) growth rate (μ).

increased up to $0.31\,\mathrm{h}^{-1}$ within 40 s, which is again very comparable with the growth rate observed after the other two pulses, and decreased after about 70 s due to the decline in $-q_S$ and $-q_{O_2}$ (Fig. 1L).

3.3. Distribution of (pseudo-steady-state) intracellular fluxes

In this study, *E. coli* central carbon metabolism was characterized at the pseudo steady-state not only by quantifying net uptake/production rates and extra-/intracellular concentrations of metabolites (see below), but also by calculation of intracellular metabolic fluxes. Metabolic flux analysis was carried out as outlined in the materials and methods section. The obtained flux distributions through central carbon metabolism are shown in Figs. 2–4.

After the *glucose pulse*, which resulted in a 2.3-fold increase in $-q_S$, the glycolytic flux increased about 2.3-fold and the

tricarboxylic acid (TCA) cycle flux about 2.5-fold. The flux entering the pentose phosphate pathway (PPP) increased only 1.4-fold, in spite of the 2.3-fold growth rate increase. The reason for this is the increased flux through NADPH dependent isocitrate dehydrogenase (ICDH) (2.5-fold).

The *pyruvate pulse* (Fig. 3) results in gluconeogenesis, evident from the reversed (negative) direction of fluxes through the glycolytic enzymes above pyruvate. The increased TCA cycle flux resulted in sufficient production of NADPH via ICDH, and therefore the flux through the oxidative PPP was assumed negligible. Gluconeogenesis is needed for the supply of glycolysis-related carbon precursors for growth (which increases about 2–3 fold). Most remarkable is that the direction of pyruvate kinase (PYK) reversed, which is plausible in *E. coli* (Keseler et al., 2009), creating most of the gluconeogenic flux. This reversal is thought to be possible by the combination of the observed very low PEP concentration (80% decrease, see below) and the expected high
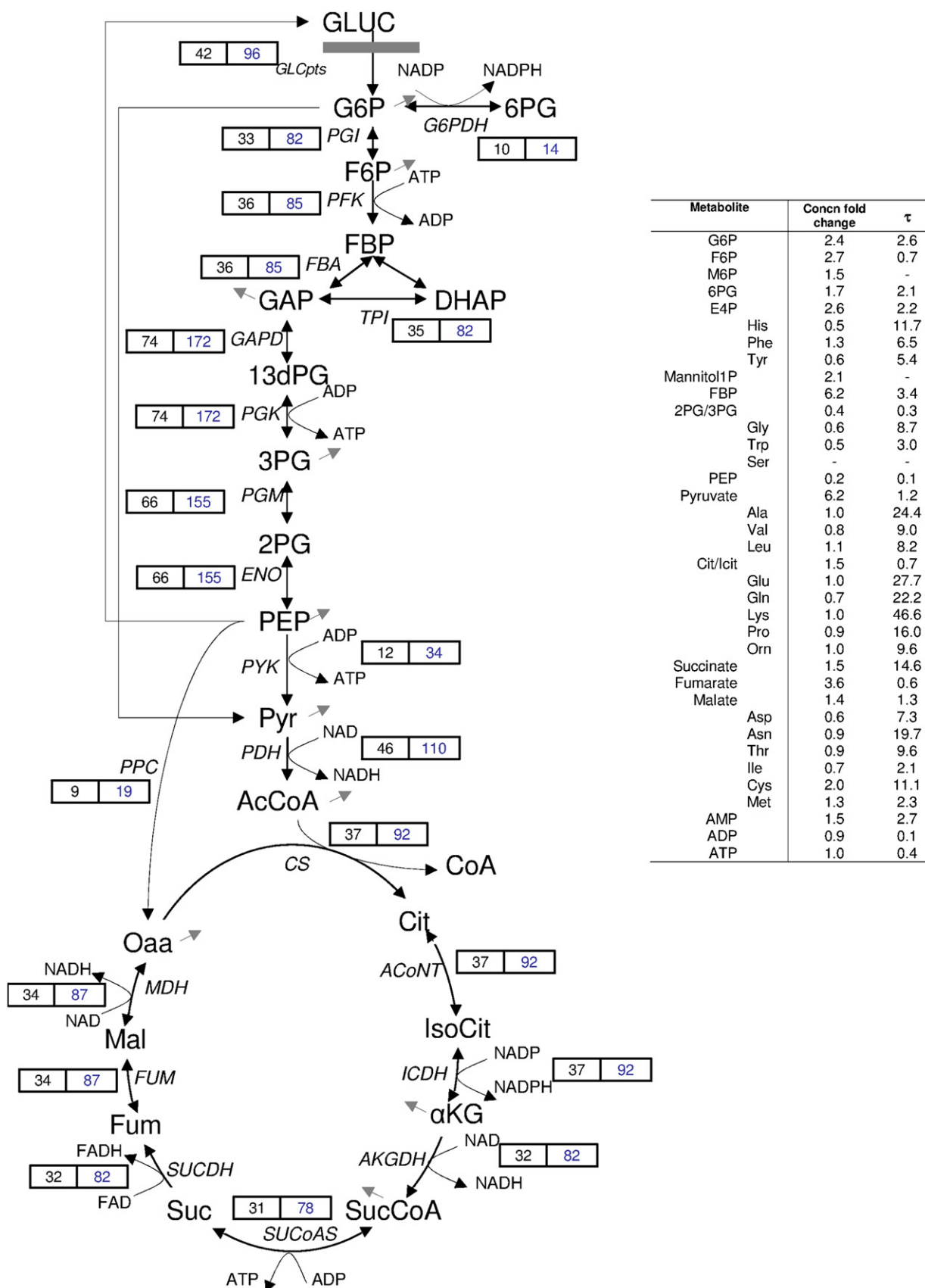
Metabolite		Concn fold change	τ
G6P		2.4	2.6
F6P		2.7	0.7
M6P		1.5	-
6PG		1.7	2.1
E4P		2.6	2.2
	His	0.5	11.7
	Phe	1.3	6.5
	Tyr	0.6	5.4
Mannitol1P		2.1	-
FBP		6.2	3.4
2PG/3PG		0.4	0.3
	Gly	0.6	8.7
	Trp	0.5	3.0
	Ser	-	-
PEP		0.2	0.1
Pyruvate		6.2	1.2
	Ala	1.0	24.4
	Val	0.8	9.0
	Leu	1.1	8.2
Cit/Icit		1.5	0.7
	Glu	1.0	27.7
	Gln	0.7	22.2
	Lys	1.0	46.6
	Pro	0.9	16.0
	Orn	1.0	9.6
Succinate		1.5	14.6
Fumarate		3.6	0.6
Malate		1.4	1.3
	Asp	0.6	7.3
	Asn	0.9	19.7
	Thr	0.9	9.6
	Ile	0.7	2.1
	Cys	2.0	11.1
	Met	1.3	2.3
AMP		1.5	2.7
ADP		0.9	0.1
ATP		1.0	0.4

Fig. 2. Metabolic reaction network and fluxes for steady-state growth on glucose and glucose pulse. *Left:* The intracellular fluxes (mmol CmolX^{-1} h^{-1}) at steady-state (glucose-limited, left box) and at pseudo-steady-state after the glucose pulse (right box). The gray arrows indicate fluxes going to biomass. *Right:* Fold change of metabolite levels at glucose pseudo-steady-state relative to the steady-state and metabolite turnover times (τ in seconds) at glucose pseudo-steady-state.
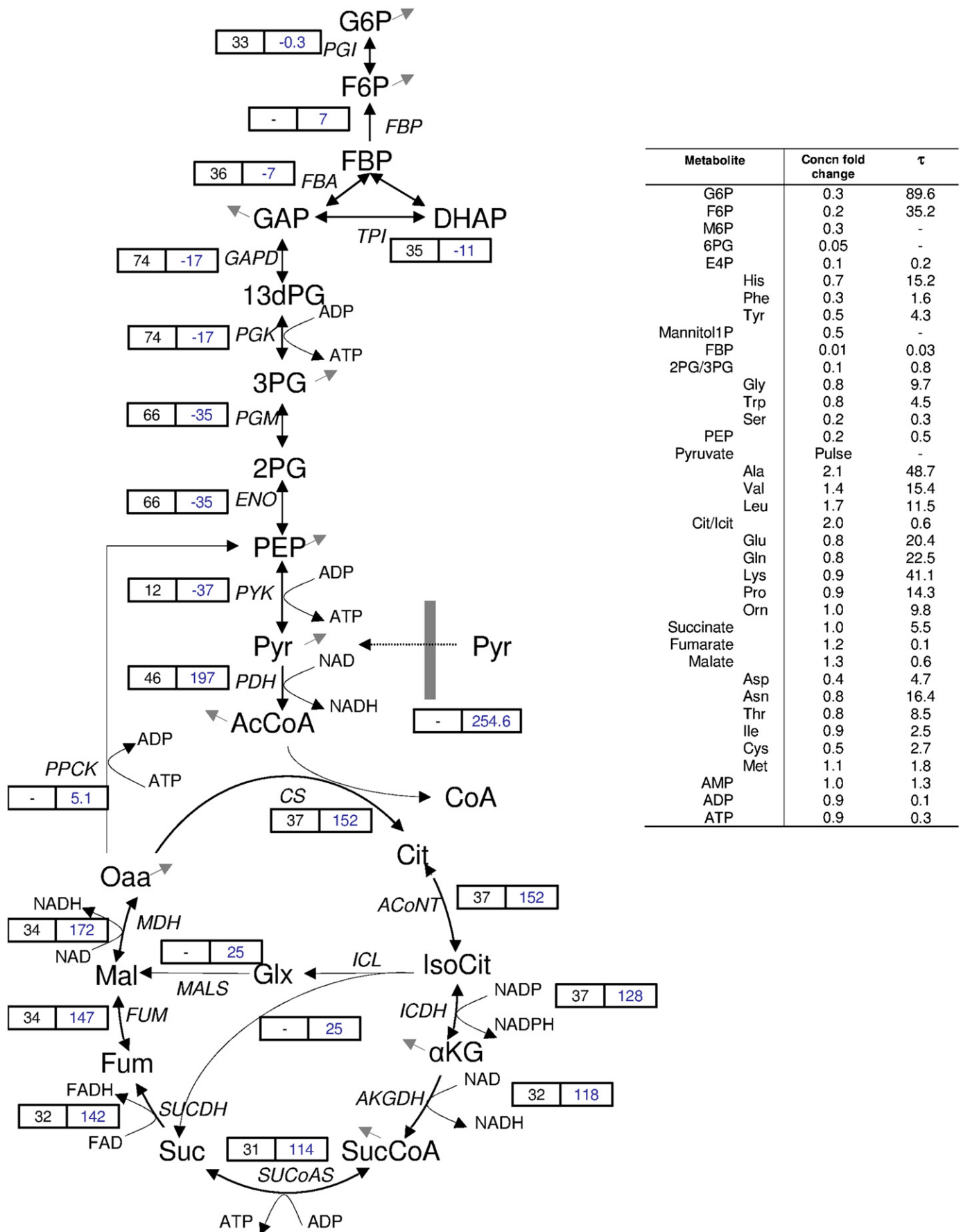
Metabolite		Concn fold change	τ
G6P		0.3	89.6
F6P		0.2	35.2
M6P		0.3	-
6PG		0.05	-
E4P		0.1	0.2
	His	0.7	15.2
	Phe	0.3	1.6
	Tyr	0.5	4.3
Mannitol1P		0.5	-
FBP		0.01	0.03
2PG/3PG		0.1	0.8
	Gly	0.8	9.7
	Trp	0.8	4.5
	Ser	0.2	0.3
PEP		0.2	0.5
Pyruvate		Pulse	-
	Ala	2.1	48.7
	Val	1.4	15.4
	Leu	1.7	11.5
Cit/Icit		2.0	0.6
	Glu	0.8	20.4
	Gln	0.8	22.5
	Lys	0.9	41.1
	Pro	0.9	14.3
	Orn	1.0	9.8
Succinate		1.0	5.5
Fumarate		1.2	0.1
Malate		1.3	0.6
	Asp	0.4	4.7
	Asn	0.8	16.4
	Thr	0.8	8.5
	Ile	0.9	2.5
	Cys	0.5	2.7
	Met	1.1	1.8
AMP		1.0	1.3
ADP		0.9	0.1
ATP		0.9	0.3

Fig. 3. Metabolic reaction network and fluxes for pyruvate pulse. *Left:* The intracellular fluxes (mmol CmolX^{-1} h^{-1}) at steady-state (glucose-limited, left box) and at pseudo-steady-state after the pyruvate pulse (right box). The gray arrows indicate fluxes going to biomass. *Right:* Fold change of metabolite levels at pyruvate pseudo-steady-state relative to the steady-state and metabolite turnover times (τ in seconds) at pyruvate pseudo-steady-state.
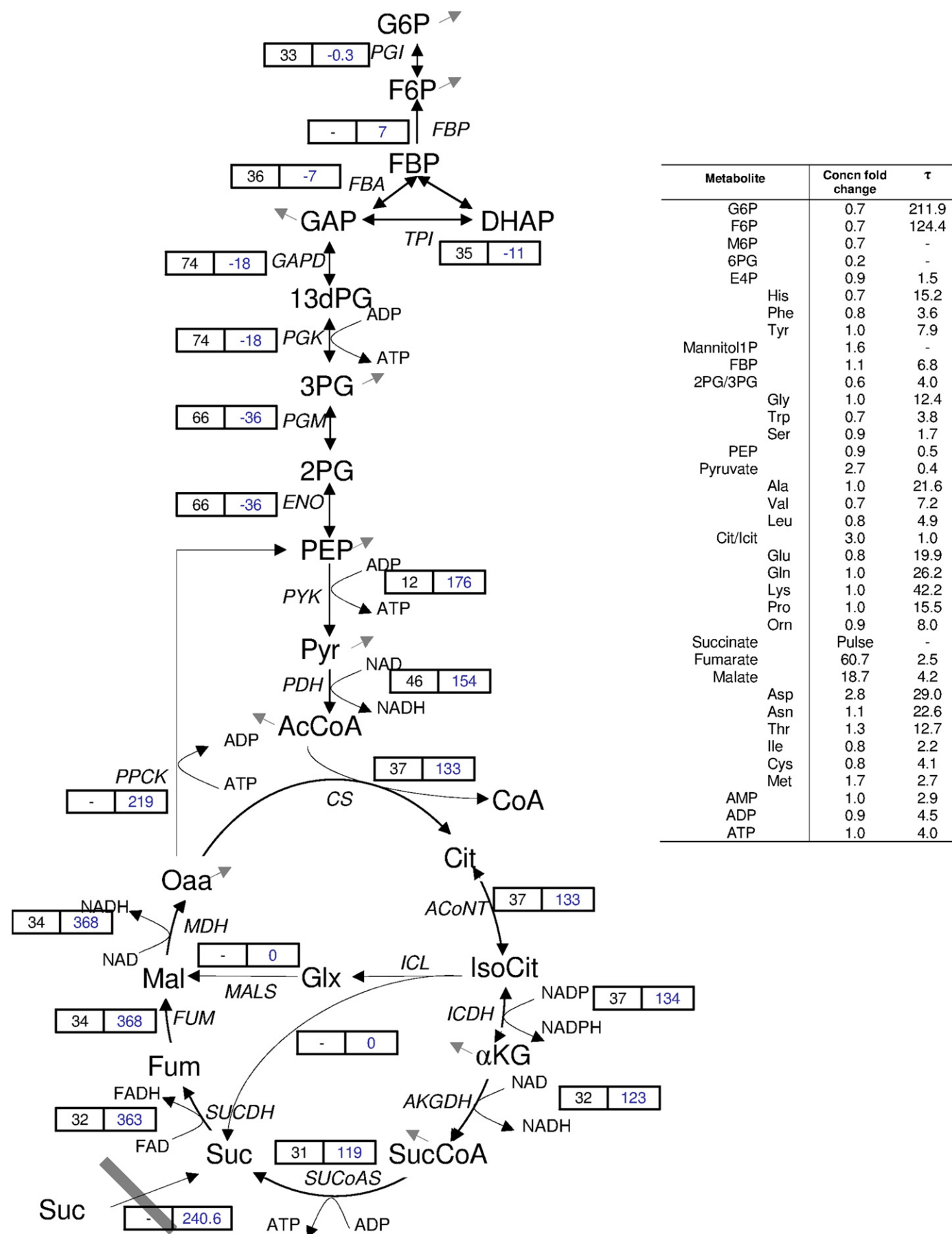
Metabolite		Concn fold change	τ
G6P		0.7	211.9
F6P		0.7	124.4
M6P		0.7	-
6PG		0.2	-
E4P		0.9	1.5
	His	0.7	15.2
	Phe	0.8	3.6
	Tyr	1.0	7.9
Mannitol1P		1.6	-
FBP		1.1	6.8
2PG/3PG		0.6	4.0
	Gly	1.0	12.4
	Trp	0.7	3.8
	Ser	0.9	1.7
PEP		0.9	0.5
Pyruvate		2.7	0.4
	Ala	1.0	21.6
	Val	0.7	7.2
	Leu	0.8	4.9
Cit/Icit		3.0	1.0
	Glu	0.8	19.9
	Gln	1.0	26.2
	Lys	1.0	42.2
	Pro	1.0	15.5
	Orn	0.9	8.0
Succinate		Pulse	-
Fumarate		60.7	2.5
Malate		18.7	4.2
	Asp	2.8	29.0
	Asn	1.1	22.6
	Thr	1.3	12.7
	Ile	0.8	2.2
	Cys	0.8	4.1
	Met	1.7	2.7
AMP		1.0	2.9
ADP		0.9	4.5
ATP		1.0	4.0

Fig. 4. Metabolic reaction network and fluxes for succinate pulse. *Left:* The intracellular fluxes (mmol CmolX^{-1} h^{-1}) at steady-state (glucose-limited, left box) and at pseudo-steady-state after the succinate pulse (right box). The gray arrows indicate fluxes going to biomass. *Right:* Fold change of metabolite levels at succinate pseudo-steady-state relative to the steady-state and metabolite turnover times (τ in seconds) at succinate pseudo-steady-state.

intracellular pyruvate concentration (which could not be quantified during the pyruvate pulse due to the large excess of extracellular pyruvate). For reversal of pyruvate kinase, thermodynamic analysis shows that the Pyr/PEP ratio should be higher than 160. In pyruvate excess conditions this value is around 50, assuming a symport mechanism for pyruvate uptake. Although the number is three fold different, considering different ΔG° values in literature and experimental measurements, this value is plausible. An alternative for pyruvate kinase might be introduction of malic enzyme, which could also act as an NADPH sink. Including malic enzyme had, however, no relevant consequences for the outcome of the MFA. The flux through pyruvate dehydrogenase (PDH) reached a value of about 200 mmol $CmolX^{-1}$ h^{-1} which was much higher than for the glucose pulse (110 mmol $CmolX^{-1}$ h^{-1}), also indicating a steeply increased intracellular pyruvate concentration. The TCA cycle flux reached a level of about 150 mmol $CmolX^{-1}$ h^{-1}, compared to 90 mmol $CmolX^{-1}$ h^{-1} after the glucose pulse.

The *succinate pulse* (as the pyruvate pulse) also gave rise to gluconeogenesis (see Fig. 4), and the flux analysis showed a high flux through the route from succinate to PEP through PEP-carboxykinase (PPCK). PEP carboxykinase has been shown to be operating in *E. coli* when grown in glucose limited chemostat cultures at a similar dilution rate as used in our experiments (0.12 h^{-1}) by Fischer and Sauer (2003), using ^{13}C metabolic flux analysis. The absolute values of the gluconeogenic flux were similar in both cases, which is due to the fact that the achieved μ was the same and the oxidative PPP was assumed to be absent in both networks. The sudden supply of succinate caused the TCA cycle flux (from succinate to oxaloacetate) to increase 11-fold (from 33 in steady-state to a maximum of around 370 mmol $CmolX^{-1}$ h^{-1} after the pulse). The TCA cycle flux from citrate to succinate increased 3.5–4-fold.

Most remarkable is the very high flux (219 mmol $CmolX^{-1}$ h^{-1}) through PPCK (PPC was assumed to be absent due to the low PEP concentration, see below). This high flux is probably realized by the very high concentration of C_4 di-acids (succinate, fumarate, malate, which form a pool in equilibrium with oxaloacetate) and low concentration of PEP (see below). The glyoxylate route is not required for succinate catabolism and was assumed to have zero flux, which is confirmed by the high concentrations of intracellular succinate and malate (see below). A much higher concentration of these products (succinate and malate) is expected to inhibit the kinetics of the isocitrate lyase (ICL) respectively malate synthase (MALS) reactions. All anaplerosis is then mediated by PPCK. In this pulse pyruvate kinase did not show inverted flux, but its flux was highly increased, in accordance with the presence of PPCK, to supply the very high TCA cycle flux.

3.4. Intracellular metabolite responses following the substrate pulses

The comparison of changes in metabolite levels (followed in two different time regimes in the BioScope, after the glucose, pyruvate and succinate pulses) is shown in Figs. 5–7. The two different broth flow rates used in the BioScope (4 mL/min and 2 mL/min providing time regimes of 0–8 s and 0–42 s, respectively) led to matching results.

After each substrate pulse, the intracellular metabolite concentrations changed dynamically, in a matching ($\sim$40 s) time frame with the changes in metabolic fluxes as expected. Just before glucose depletion (275 s) the accumulated carbon in the measured metabolite pools represents about 20% of the added glucose amount (see Supplementary Information Section 6), which is in agreement with our previous glucose pulse findings (Taymaz-Nikerel et al., 2011).

The fold changes in metabolite pss concentrations relative to the steady-state are given in the right panels of the Figs. 2–4, together with the turnover times of the pss pools. For many metabolites the turnover times are in the order of seconds, which shows that, even in the transient period of 40 s, the system can be approximated as being in flux-pseudo-steady-state, thus allowing a simple pseudo-steady-state flux calculation during the transient.

The intracellular metabolite dynamic patterns after the glycolytic glucose pulse were, as was partly discussed by De Mey et al. (2010), similar to our previous work (Taymaz-Nikerel et al., 2011). The intracellular levels of the adenine nucleotides and thus the adenylate energy charge of the cells are high and do not change significantly after any of the given substrate pulses (Fig. 5).

The intracellular concentrations of the upper glycolytic metabolites and Mannitol1P increased (2–6 fold) after the glucose pulse, most probably because of the increased glycolytic flux (2.3-fold increase in $-q_S$). After the succinate and pyruvate pulses, the concentrations of the upper glycolytic metabolites decreased (Fig. 6) due to the absence of external glucose flux and occurrence of flux reversal by gluconeogenesis. The steep decrease of G6P and F6P concentrations during the pyruvate and succinate pulses was accompanied by a near collapse of the 6PG pool, strongly suggesting the absence of the oxidative PPP (as assumed for the flux calculations in Figs. 3 and 4).

Presence of the PPCK facilitated the gluconeogenesis after the succinate pulse due to its high flux. This high flux through PPCK is due to the high influx of succinate and low levels of PEP, which created a thermodynamic driving force in the direction of gluconeogenesis. The observed increase of the intracellular pyruvate level (2.7-fold) after the succinate pulse (Fig. 6) is also in agreement with the increased PPCK flux (Fig. 4), although the increase was much smaller compared to the glucose pulse (6.2-fold), due to the absence of PTS activity during the succinate pulse.

The intracellular amino acids showed also fast dynamic responses, however, with very moderate (less than 2-fold) changes of their concentrations. In most cases the amino acid levels followed the changes in their precursors (Supplementary Figs. 7–10). Examples are the increase in pyruvate-derived amino acids such as alanine (2.1-fold), leucine (1.7-fold) and valine (1.4-fold) following the increase in pyruvate (Supplementary Fig. 8). Another example for this precursor-related response of amino acid levels is the decrease in leucine and valine (20% and 30%) after the succinate pulse with a much more delayed response compared to the glucose pulse (Supplementary Fig. 8). The aspartate level was increased 2.8-fold after the succinate pulse (Supplementary Fig. 10) and could be indicative for an increased oxaloacetate level (not measured), due to the large increase in the intracellular levels of the preceding C_4 acid metabolites (malate: $\sim$19-fold, fumarate: $\sim$61-fold).

3.5. The profiles of reaction quotients and flux directions

The reaction quotient Q of a reaction (also known as mass action ratio) can be directly calculated from the measured metabolite levels and the reaction stoichiometry (see Section 2). Comparison with the equilibrium constant indicates whether a reaction operates close to equilibrium or not. Information on changes in Q (as a function of time) gives insight in the direction of a reaction in the cell: $Q/K_{eq} < 1$ forward, $Q/K_{eq} = 1$ equilibrium, and $Q/K_{eq} > 1$ backward. Recently, Canelas et al. (2011) showed in *S. cerevisiae* that Q and flux are linearly correlated for near-equilibrium reactions. This is of importance because in that case two independent quantities, measured intracellular metabolite
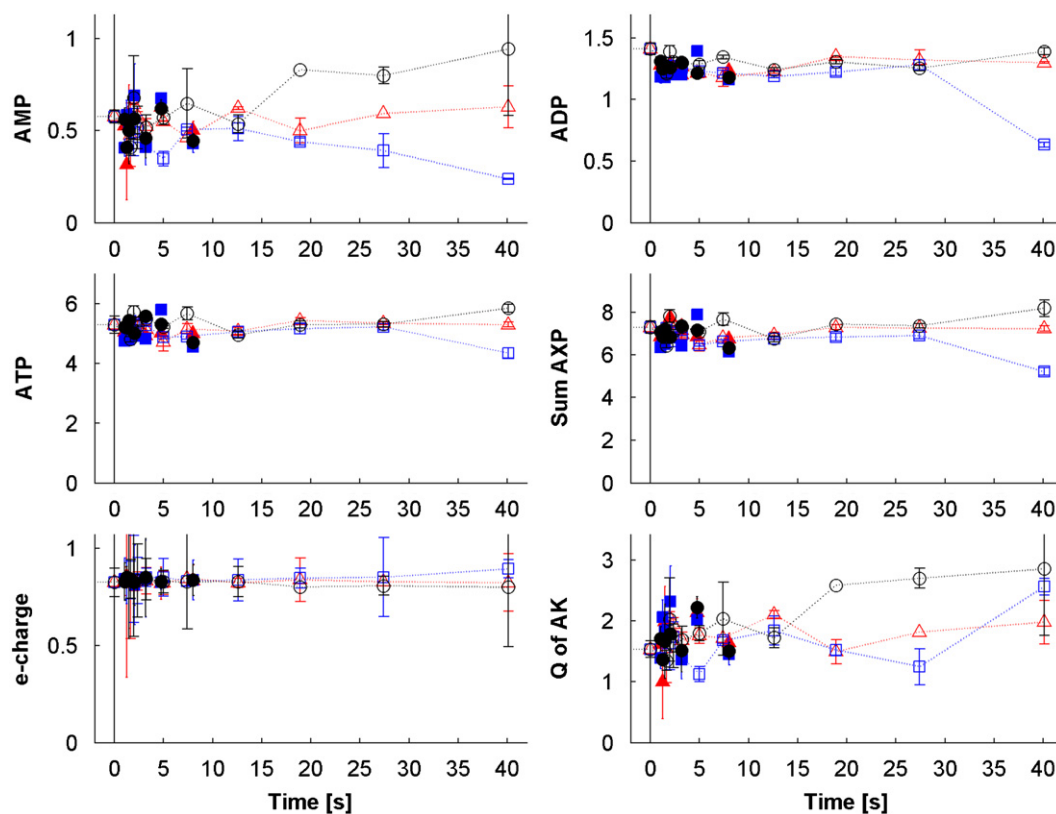
Fig. 5. Measured adenine nucleotides (μmol/g DW), sum of AXP (μmol/g DW), energy charge ($-$) and Q of AK ($2ADP \leftrightarrow AMP + ATP$) ($-$) during the glucose (circles), pyruvate (squares) and succinate (triangles) pulse. Open symbols are at flow rate$=2$ mL/min, closed symbols are at flow rate$=4$ mL/min. ADP and ATP patterns during the glucose pulse are from De Mey et al. (2010).
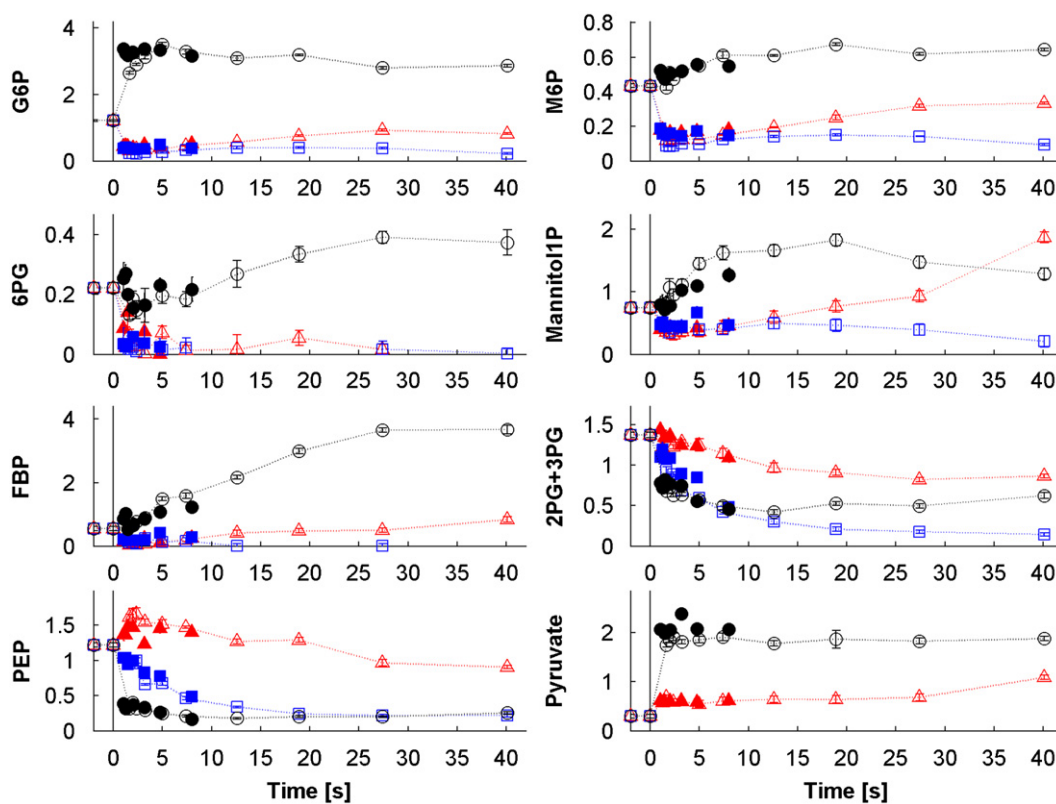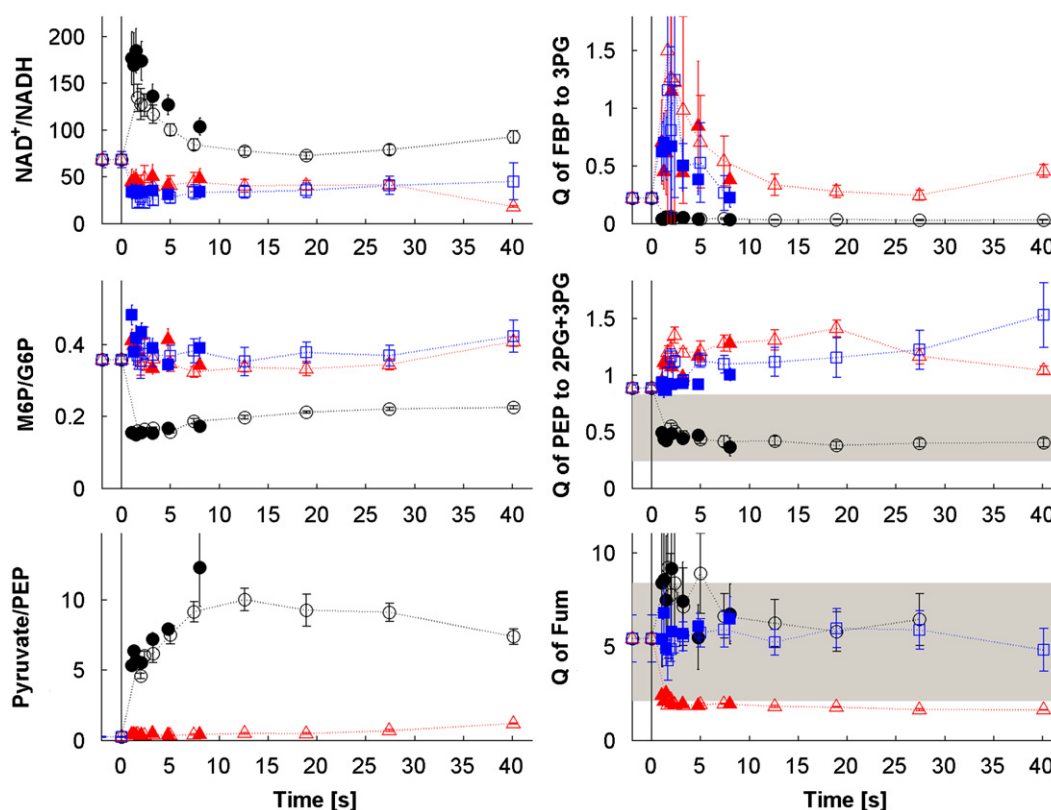

Fig. 6. Measured amounts of upper glycolytic metabolites, 6PG, Mannitol1P, lower glycolytic metabolites (μmol/g DW) during the glucose (circles, De Mey et al., 2010), pyruvate (squares) and succinate (triangles) pulses. Open symbols are at flow rate$=2$ mL/min, closed symbols are at flow rate$=4$ mL/min.

Fig. 7. Some relevant reaction quotients and metabolite ratios during the glucose (circles), pyruvate (squares) and succinate (triangles) pulses. Open symbols are at flow rate=2 mL/min, closed symbols are at flow rate=4 mL/min. Q of PEP to (2 PG + 3 PG) and Pyruvate/PEP patterns during the glucose pulse are from De Mey et al. (2010). Gray shaded areas show the published K_{eq} range.

levels (represented by Q) and calculated metabolic fluxes (v), can be compared (see below).

According to our flux analysis, the pyruvate and succinate pulses resulted in a change in the direction of the glycolytic reactions (see Fig. 7). This is confirmed by the observed changes in the Q values for M6P/G6P, FBP to 3PG and PEP/(2PG+3PG), which increased immediately above their equilibrium constant, indicative of the flux reversal needed for the occurrence of gluconeogenesis.

The Q of fumarase decreased in the succinate pulse (Fig. 7), providing more driving force for this reaction and confirms the calculated more than 11-fold increased TCA flux from succinate to Oaa (Fig. 4).

The cytosolic redox potential, i.e., NAD$^+$/NADH ratio increased after the glucose pulse and returned back to the steady-state value in 20 s (Fig. 7). However, in contrast to the glucose pulse, the NAD$^+$/NADH ratio decreased after the succinate and pyruvate pulses (Fig. 7), which also confirmed the reversal of glycolytic flux.

3.6. "Q-linear kinetics" of central carbon metabolism

In this study, we show that central metabolism of E. coli, challenged with three different substrate pulses, is highly flexible and can accommodate large changes in fluxes and metabolite concentrations in a time frame of seconds. These changes (including reversal of flux direction) in metabolic fluxes correspond qualitatively to the observed large changes in the intracellular concentrations of metabolites, leading to expected changes in Q-values (supporting flux reversal and/or large flux changes) of all near reversible reactions. It is now of interest to apply a quantitative, recently introduced kinetic concept (Canelas et al., 2011), where for a certain reaction the Q-value is plotted against the

reaction rate (v). In such a plot the x-intercept gives the maximum in vivo forward reaction rate of the corresponding enzyme whereas the y-intercept gives an estimate of the in vivo equilibrium constant of the reaction, K_{eq}. When the obtained Q range is of the same order of magnitude as the reported in vitro K_{eq} value of the reaction, the reaction can be classified as operating at pseudo-equilibrium or near-equilibrium. It has been reported that 75% of the reactions in central metabolism of aerobically grown S. cerevisiae behaved as pseudo/near equilibrium, while for the near-equilibrium reactions a linear decrease of Q with v has been observed (Canelas et al., 2011).

In our E. coli pulse experiments (with glucose/pyruvate/succinate) the reactions catalyzed by fumarase and enolase, the lumped reaction from FBP to 3PG and pyruvate kinase revealed a linear decrease of Q vs. flux of the catalyzed reaction (see Fig. 8), showing near-equilibrium behavior. It should be noted that in several Q(v) plots the sign of v changes (due to the shift to gluconeogenesis).

In the work of Canelas et al. (2011), $K_{ENO} \times K_{GPM}=0.46$ was found to be lower than our value of 1.05 (Fig. 8), which is slightly higher than the range of published in vitro data at pH 7 (Table 1). For the lumped reaction from FBP to 3PG, literature K_{eq}-data shows a very broad range covering several orders of magnitude (Table 1). The value of K_{eq} we determined for E. coli is close to the lower end of the range (Table 1) as also found by Canelas et al. (2011) in S. cerevisiae, again suggesting that this part of glycolysis operates near-equilibrium.

Pyruvate kinase was classified as far-from-equilibrium by Canelas et al. (2011), although it is known to be a reversible reaction (Keseler et al., 2009). Our results also indicate that this reaction reverses during the pseudo-steady-state conditions after the pyruvate pulse (gluconeogenesis). Presently, K_{eq} is found to be
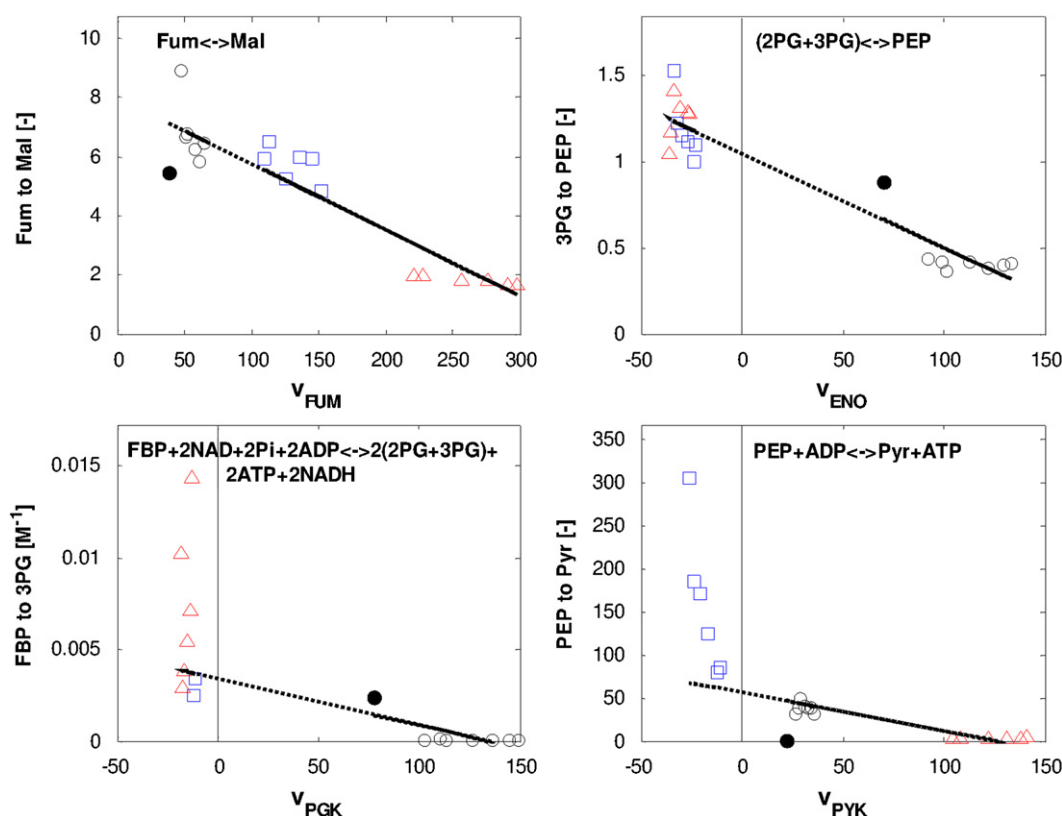
Fig. 8. Q vs. flux (v in mmol CmolX^{-1} h^{-1}) plots (near-equilibrium reactions) during the glucose (circles), pyruvate (squares) and succinate (triangles) pulses. Closed circle is the steady-state before the pulse.

Table 1
Comparison of y-intercept of $Q(v)$ plots in *E. coli* to literature K_{eq} range and *in vivo* derived K_{eq} in *S. cerevisiae* (Canelas et al. 2011).

Enzyme	Literature K_{eq} range pH$\sim$7	*In vivo* K_{eq} (*S. cerevisiae*)	Our study y-intercept
FUM	2.10–8.40	5.18 ± 0.14	8.00
PGM+ENO	0.24–0.83	0.46 ± 0.01	1.05
FBA+TPI+GAPD+PGK, (M^{-1})	0.002–100.9	0.0052 ± 0.0005	0.0034
PYK	6451.6	–	56.3

56.3, which is two orders of magnitude lower than the published value of about 6400 (Table 1).

The fumarase catalyzed reaction showed, as expected, a lower Q with higher flux after the gluconeogenic pyruvate and succinate pulses. The observed K_{eq} for fumarase in *E. coli* is 8.0 (Table 1), which is higher than the value of 5.2 observed in *S. cerevisiae* (Canelas et al., 2011), but still within the range of published *in vitro* data (Table 1). The *in vivo* v^{max} of fumarase is found to be $\sim$360 mmol CmolX^{-1} h^{-1} (x-intercept in Fig. 8), which is close to the calculated flux of 368 mmol CmolX^{-1} h^{-1} at succinate excess pseudo-steady-state conditions (see Fig. 4).

4. Discussion

We have applied three different substrate pulses (glucose, pyruvate and succinate) to glucose limited chemostat cultures of *E. coli*. Remarkably, after each different substrate pulse, the growth rate was observed to increase with more than a factor two to a similar value of 0.3 h^{-1}, which was well below μ^{max}.

We carried out metabolome and metabolic flux analysis during the short term, highly dynamic transient and the subsequent pseudo steady state. The integration of the obtained results gave us novel insights into the flexibility of the metabolic network. Moreover, our work shows that not only coupling flux data to concentrations of metabolites is possible, but also the directions of the reactions can be inferred from intracellular concentration data (*i.e.*, via the mass action ratio, or Q-value). Additionally, the information on intracellular fluxes and metabolite concentrations can be used to deduce *in vivo* kinetic parameters of reactions in *E. coli* through the application of a thermodynamically inspired kinetic approach, namely Q-linear kinetics.

4.1. Steady-state: Reproducibility and recovery after substrate pulses

Tightly controlled glucose limited steady-state chemostat conditions were used as well-defined initial state for our rapid substrate pulse experiments. For the substrate pulses carried out in the chemostat it was found that after each perturbation the steady-state was completely recovered, in terms of metabolite

levels (see Supplementary Table 3) and fluxes. This indicates that possible changes of enzyme levels in central metabolism during the pulse can be considered negligible in the total time frame of the pulse experiment (~900 s). The observation that over a period of 50–100 h of chemostat cultivation of *E. coli*, covering 7–14 residence times or 10–20 generations, the metabolite levels do not significantly change (see Supplementary Table 3) is different from what was reported for *Saccharomyces cerevisiae* (Mashego et al., 2005), where intracellular metabolite levels significantly changed within 15–20 generations of chemostat cultivation.

4.2. Specific growth rate increased from 0.13 h⁻¹ to ~0.3 h⁻¹ within 30–40 s after pulses with different substrates

E. coli cells, grown in aerobic glucose-limited chemostats at $\mu = 0.13\ h^{-1}$, were subjected to three different substrate pulses. After each pulse (glucose, pyruvate and succinate), a pseudo-steady-state was achieved in about 30–40 s after the pulse, whereby the growth rate increased to a similar value of 0.3 h⁻¹. This growth rate was calculated based on the measured $-q_S$ and $-q_{O_2}$.

Also in earlier studies, using a step-up in the dilution rate of carbon limited chemostat cultures, a very rapid increase of the growth rate was reported (Mateles et al., 1965; Yun et al., 1996).

From totally different additional information, namely the turnover times of amino acid pools, the calculated 2–3 fold increase in the growth rate is supported: The turnover times of amino acids, being several tens of seconds (calculated at the steady-state before the pulse, see Supplementary Table 4), are not in line with the fast amino acid response observed (< 10 s, Supplementary Figs. 7–10). This discrepancy can be explained by the boost in the growth rate (2–3 fold), which leads to a fast and 2–3 fold increase in the amino acid consumption rate and hence a fast increase in the flux through the amino acid synthesis pathways leading to the observed lower turnover times in the pseudo-steady-state (see Figs. 2–4).

The observed increase in μ from 0.13 h⁻¹ to 0.3 h⁻¹ as response to all three substrate pulses raises two questions. The first question is why μ does not increase beyond 0.3 h⁻¹. An obvious reason could be a limited capacity to generate ATP, due to a maximal oxygen uptake capacity. It was indeed observed that after the glucose and pyruvate pulses a similar value of the specific oxygen consumption rate was reached (Fig. 1C and 1G). However, as response to the succinate pulse, the oxygen consumption rate increased to a much higher value (~500 mmol O₂ CmolX⁻¹ h⁻¹). This value corresponds with the maximal oxygen uptake rate observed for the present strain (~500 mmol CmolX⁻¹ h⁻¹ when grown in unlimited batch cultures with $\mu^{max} \sim 0.6\ h^{-1}$) and the reported maximum specific oxygen uptake rate for *E. coli* of 20 mmol O₂/gDW/h (~500 mmol O₂ CmolX⁻¹ h⁻¹) (Carlson and Srienc, 2004). The observed rapid increase to the maximum O₂ uptake rate indicates that the capacity limit of the electron transport chain is independent of the growth rate at which *E. coli* is cultivated, being similar at $\mu = 0.13\ h^{-1}$ (chemostat) and $\mu \sim 0.6\ h^{-1}$ (batch). Energy production is therefore not likely to be a limiting factor for growth.

A second candidate could be a limit of the protein synthesis capacity. It is well known that the ribosome content of *E. coli* depends strongly on the growth rate (Dennis and Bremer, 1974). However, it has been reported that at low growth rates the ribosome content is higher than required for protein synthesis (Koch and Deppe, 1971; Nierlich, 1974; Yun et al., 1996). Koch and Deppe observed, using ¹⁴C labeling experiments, that this ribosomal overcapacity allowed for an instantaneous increase in protein synthesis rate after a shift-up in dilution rate in a glucose limited chemostat culture. It could therefore be that the ribosome

content of cells grown at $\mu = 0.13\ h^{-1}$ is just sufficient to reach a growth rate μ of 0.3 h⁻¹. The observed fast increase in growth rate then requires that the protein production rate at the ribosomes is rapidly increased with a factor 2–3.

Now the important question remains what the kinetic trigger is which is responsible for this fast increase of the ribosomal activity. Obvious candidates are increased availabilities of amino acids and ATP. However, our data show that the sum of the intracellular levels of amino acids after the three pulses is slightly lower (factor 0.90, 0.81 and 0.94 for the glucose, pyruvate and succinate pulses respectively) and that the AXP levels are practically constant after the pulse.

Another possibility to explain the sudden increased protein synthesis rate is that the transcript levels for all proteins increase 2–3 fold within about 30 s. This seems unlikely, although, to our best knowledge the earliest transcript measurements after perturbations of *E. coli* cells have only been conducted after a few minutes (Blanchard et al., 2007; Durfee et al., 2008; Partridge et al., 2006; Trotter et al., 2011). For glucose perturbations in *S. cerevisiae*, it has been reported that the first changes in transcript levels occur 2 min after the perturbation (Kresnowati et al., 2006).

Nevertheless, perturbation induced changes in the levels of central metabolites could act as signal(s) to global transcription factors for increased transcription. In *E. coli* FBP is known to inactivate the global transcription factor Cra. Hardiman et al. (2010) showed the impact of changes in the FBP level in relation to Cra on the transcription of central carbon metabolism genes and the effect of these changes on the metabolic fluxes. Furthermore, Schaub and Reuss (2008) have shown a positive correlation between the intracellular FBP concentration and the growth rate of *E. coli* cells grown in glucose limited chemostat cultures. If an increase of the intracellular FBP concentration would be the trigger for increase of the growth rate, we would expect to observe such an increase after each of the three substrate pulses. However, although we observed an up to 6 fold increase in FBP as response to the glucose pulse, both the pyruvate and succinate pulses did not result in an increase of the FBP level, but, on the contrary, to a significant decrease. Hardiman et al. (2010) argued that a decrease of the level of FBP could be a signal for reduced specific growth rate. Our findings clearly contradict the assumed regulatory role of FBP, because in our experiments the observed increase in the growth rate did not have any relation with the measured intracellular FBP level.

In conclusion, it appears that the observed rapid increase of the growth rate and thus of the protein production rate, as response to the different substrate pulses, is triggered by a yet unknown mechanism.

4.3. Fluxome and metabolome are flexible and strongly correlated: Q-values and Q(ν) relation

Our results reveal that the intracellular metabolic network of *E. coli* is remarkably flexible. The different flux values observed after each pulse give insight in the behavior of metabolites under different conditions, most important being the immediate occurrence of gluconeogenesis after the pyruvate and succinate pulses due to the reversible reactions. Although in the network, due to the same increase in μ, the pyruvate and succinate pulses led to the same gluconeogenic flux, there are also major differences between the two pulses. Most significant are the calculated reversal of PYK during the pyruvate pulse, the extreme increase in the TCA cycle flux between succinate and Oaa and the relatively high PPCK flux during the succinate pulse. It is well known (Lowry et al., 1971) that when *E. coli* cells are grown on succinate, phosphoenolpyruvate carboxykinase (Ppck) converts

oxaloacetate to PEP, which then diverges to gluconeogenesis and to the formation of pyruvate (to feed the TCA cycle) as indicated in our flux pattern (Fig. 4). In contrast to the intracellular flux distributions, the intracellular levels of adenine nucleotides and thus the adenylate energy charge of the cells did not change significantly after any of the pulsed substrates (Fig. 5). This shows, considering the very large changes in O_2-uptake rates (up to a factor 5 in 40 s), the robustness and effective coupling of the energy system in E. coli.

Additionally, the fact that the cells use the supplied extra carbon for energy production and for growth only, and not for by-product secretion, might indicate that this global flexibility towards growth has a functional (competitive) importance through the onset of efficient and fast cell growth upon the sudden relief of substrate limitation. Ishii et al. (2007) demonstrated the robustness of the metabolic network of E. coli against genetic and environmental perturbations at the level of gene and protein expression. With the demonstrated flexibility of fluxes/metabolites/growth rate, E. coli has been shown to react rapidly ($\sim$40 s) and efficiently (2–3 fold higher μ, high biomass yield, and no by-products) to the imposed environmental changes.

Calculated metabolic flux patterns were supported by measured changes in metabolite levels and new insights into the central carbon metabolism of E. coli were gained. Integration of fluxome and metabolome data revealed solid relationships between the changes at these two levels, as shown quantitatively by the change in Q-values and the $Q(v)$ relation. Most of the above mentioned flux changes/inversions could be related to changes in the thermodynamic driving force as quantified in the reaction quotients Q. Also for several reactions the Q-linear kinetic format appears to apply, as found previously in S. cerevisiae (Canelas et al., 2011). The flux term should be preferably expressed as flux per amount of enzyme, but since in our experimental design enzyme levels can be considered constant (due to the short duration of the pulse experiments), it was appropriate to use absolute fluxes. Accurate determination of in vivo K_{eq} requires including conditions where the fluxes approach zero or even invert their direction, as was the case here. The obtained K_{eq} values are close to the ones reported by Canelas et al. (2011). The reactions from FBP to 3 PG, enolase and fumarase were classified as near-equilibrium under in vivo conditions here and in S. cerevisiae (Canelas et al., 2011). Importantly, for the lumped reaction from FBP to 3 PG the assumed concentration of inorganic phosphate (Pi) has a big effect on the final K_{eq}. Here, a Pi concentration of 50 mM was assumed, however, if the actual Pi concentration would be 10 times lower, K_{eq} would increase a factor of 100, which is, however, still in the published range (Table 1). The presently found lower K_{eq} value (compared to the published one) for pyruvate kinase indicates a possible difference between in vivo and in vitro conditions.

The estimated in vivo v^{max} of fumarase was found to be close to the flux at succinate excess pseudo-steady-state conditions (Fig. 4). This shows that the cells might have reached their maximal TCA cycle capacity after the succinate pulse, as was also observed for the O_2 uptake rate.

The NAD^+/NADH ratio showed distinct profiles for the different substrate pulses, an increase after the glucose pulse and a decrease after the succinate and pyruvate pulses (Fig. 7). This decrease is in agreement with the occurrence of gluconeogenesis, which consumes NADH. Also from a Q-linear kinetics perspective a decrease of the NAD^+/NADH ratio provides the driving force for flux reversal around GAPDH required for gluconeogenesis.

Based on the results of the application of Q-linear kinetics, we expect that characterization of intracellular fluxes and metabolites under various conditions using this kinetic concept will be an important tool in microbial systems biology in the future.

4.4. Comparison to previous published work

The sudden supply of additional carbon to glucose limited chemostat grown cells was used to generate energy, which could be inferred from the observed significant increase in the specific oxygen consumption rate of the cells, to produce biomass and to accumulate intracellular metabolites, as no by-products were formed during the three different substrate pulses. Link et al. (2010) also have carried out comparable substrate pulses using glucose, pyruvate and succinate to aerobic glucose-limited fed-batch grown (μ=0.1 h^{-1}) E. coli cells. In contrast to our findings, they observed acetate and formate excretion after transferring the cells from fed-batch to unlimited batch conditions, with glucose and pyruvate as substrates. For succinate as substrate fumarate and α-ketoglutarate secretion was observed. The production of these by-products might be due to the use of a different strain and/or the much higher (7–17 fold) concentrations of substrates supplied ($\sim$43 mM glucose, $\sim$42 mM pyruvate, and $\sim$28 mM succinate). Unfortunately, Link et al. (2010) did not show measurements of the dissolved oxygen concentration during the transients. Furthermore they did not indicate whether they had taken measures to prevent the occurrence of oxygen limitation during the perturbation experiments (e.g. by supplying O_2-enriched air). It can therefore not be excluded that O_2-limitation may have caused the formation of by-products during these perturbation experiments. That oxygen limitation can result in immediate by-product formation in glucose limited E. coli cells has been demonstrated by Sunya et al. (2012), who clearly showed that acetate and formate were formed after glucose pulses of different intensities to glucose-limited chemostat cultures at dilution rate of 0.15 h^{-1}, with concomitant oxygen limitation.

Despite these differences, comparable results were observed in the changes of intracellular metabolite concentrations presented by Link et al. (2010) although their measurements only started after 120 s and they presented only four pss intracellular metabolite pools. They showed that the G6P+F6P and FBP pools increased during glucose excess and decreased during glucose depletion and pyruvate and succinate excess, while the decrease was more pronounced during pyruvate excess. The malate concentration increased to a much higher level during succinate excess compared to glucose and pyruvate excess. All this agrees qualitatively well with our findings.

Appendix A. Supporting information

Supplementary data associated with this article can be found in the online version at http://dx.doi.org/10.1016/j.ymben.2013.01.004.

References

Blanchard, J.L., Wholey, W.Y., Conlon, E.M., Pomposiello, P.J., 2007. Rapid changes in gene expression dynamics in response to superoxide reveal SoxRS-dependent and independent transcriptional networks. PLoS One 2 (11), e1186.

Canelas, A., Ras, C., Ten Pierick, A., van Gulik, W., Heijnen, J., 2011. An *in vivo* data-driven framework for classification and quantification of enzyme kinetics and determination of apparent thermodynamic data. Metab. Eng. 13 (3), 294–306.

Carlson, R., Srienc, F., 2004. Fundamental *Escherichia coli* biochemical pathways for biomass and energy production: creation of overall flux states. Biotechnol. Bioeng. 86 (2), 149–162.

Chassagnole, C., Noisommit-Rizzi, N., Schmid, J.W., Mauch, K., Reuss, M., 2002. Dynamic modeling of the central carbon metabolism of *Escherichia coli*. Biotechnol. Bioeng. 79 (1), 53–73.

De Mey, M., Taymaz-Nikerel, H., Baart, G., Waegeman, H., Maertens, J., Heijnen, J.J., van Gulik, W.M., 2010. Catching prompt metabolite dynamics in *Escherichia coli* with the BioScope at oxygen rich conditions. Metab. Eng. 12 (5), 477–487.

Dennis, P.P., Bremer, H., 1974. Macromolecular composition during steady-state growth of *Escherichia coli* B/r. J. Bacteriol. 119 (1), 270–281.

Durfee, T., Hansen, A.M., Zhi, H., Blattner, F.R., Jin, D.J., 2008. Transcription profiling of the stringent response in *Escherichia coli*. J. Bacteriol. 190 (3), 1084–1096.

Fiehn, O., 2001. Combining genomics, metabolome analysis, and biochemical modelling to understand metabolic networks. Comp. Funct. Genomics 2 (3), 155–168.

Fischer, E., Sauer, U., 2003. A novel metabolic cycle catalyzes glucose oxidation and anaplerosis in hungry *Escherichia coli*. J. Biol. Chem. 278 (47), 46446–46451.

Gutowski, S.J., Rosenberg, H., 1975. Succinate uptake and related proton movements in *Escherichia coli* K12. Biochem. J. 152 (3), 647–654.

Hardiman, T., Meinhold, H., Hofmann, J., Ewald, J.C., Siemann-Herzberg, M., Reuss, M., 2010. Prediction of kinetic parameters from DNA-binding site sequences for modeling global transcription dynamics in *Escherichia coli*. Metab. Eng. 12 (3), 196–211.

Heinemann, M., Sauer, U., 2010. Systems biology of microbial metabolism. Curr. Opin. Microbiol. 13 (3), 337–343.

Ishii, N., Nakahigashi, K., Baba, T., Robert, M., Soga, T., Kanai, A., Hirasawa, T., Naba, M., Hirai, K., Hoque, A., et al., 2007. Multiple high-throughput analyses monitor the response of *E. coli* to perturbations. Science 316 (5824), 593–597.

Keseler, I.M., Bonavides-Martinez, C., Collado-Vides, J., Gama-Castro, S., Gunsalus, R.P., Johnson, D.A., Krummenacker, M., Nolan, L.M., Paley, S., Paulsen, I.T., et al., 2009. EcoCyc: a comprehensive view of *Escherichia coli* biology. Nucleic Acids Res. 37, D464–D470.

Kim, T.Y., Kim, H.U., Lee, S.Y., 2010. Data integration and analysis of biological networks. Curr. Opin. Biotechnol. 21 (1), 78–84.

Koch, A.L., Deppe, C.S., 1971. *In vivo* assay of protein synthesizing capacity of *Escherichia coli* from slowly growing chemostat cultures. J. Mol. Biol. 55 (3), 549–562.

Kresnowati, M.T., van Winden, W.A., Almering, M.J., ten Pierick, A., Ras, C., Knijnenburg, T.A., Daran-Lapujade, P., Pronk, J.T., Heijnen, J.J., Daran, J.M., 2006. When transcriptome meets metabolome: fast cellular responses of yeast to sudden relief of glucose limitation. Mol. Syst. Biol. 2, 49.

Lang, V.J., Leystralantz, C., Cook, R.A., 1987. Characterization of the Specific Pyruvate Transport System in *Escherichia coli* K-12. J. Bacteriol. 169 (1), 380–385.

Liao, J.C., 1993. Modelling and analysis of metabolic pathways. Curr. Opin. Biotechnol. 4 (2), 211–216.

Link, H., Anselment, B., Weuster-Botz, D., 2010. Rapid media transition: an experimental approach for steady state analysis of metabolic pathways. Biotechnol. Prog. 26 (1), 1–10.

Lowry, O.H., Carter, J., Ward, J.B., Glaser, L., 1971. The effect of carbon and nitrogen sources on the level of metabolic intermediates in *Escherichia coli*. J. Biol. Chem. 246 (21), 6511–6521.

Mashego, M.R., Jansen, M.L., Vinke, J.L., van Gulik, W.M., Heijnen, J.J., 2005. Changes in the metabolome of *Saccharomyces cerevisiae* associated with evolution in aerobic glucose-limited chemostats. FEMS Yeast Res. 5 (4-5), 419–430.

Mateles, R.K., Ryu, D.Y., Yasuda, T., 1965. Measurement of unsteady state growth rates of micro-organisms. Nature 208 (5007), 263–265.

Nasution, U., 2007. A dynamic and steady state metabolome study of central metabolism and its relation with the penicillin biosynthesis pathway in *Penicillium chrysogenum*. PhD Thesis. Delft University of Technology, Delft.

Nielsen, J., 2001. Metabolic engineering. Appl. Microbiol. Biotechnol. 55 (3), 263–283.

Nierlich, D.P., 1974. Regulation of bacterial growth. Science 184 (4141), 1043–1050.

Nikerel, I.E., van Winden, W.A., van Gulik, W.M., Heijnen, J.J., 2006. A method for estimation of elasticities in metabolic networks using steady state and dynamic metabolomics data and linlog kinetics. BMC Bioinf. 7, 540.

Nikerel, I.E., van Winden, W.A., Verheijen, P.J., Heijnen, J.J., 2009. Model reduction and a priori kinetic parameter identifiability analysis using metabolome time series for metabolic reaction networks with linlog kinetics. Metab. Eng. 11 (1), 20–30.

Oldiges, M., Takors, R., 2005. Applying metabolic profiling techniques for stimulus–response experiments: chances and pitfalls. Technol. Transfer Biotechnol. Lab. Ind. Prod. 92, 173–196.

Partridge, J.D., Scott, C., Tang, Y., Poole, R.K., Green, J., 2006. *Escherichia coli* transcriptome dynamics during the transition from anaerobic to aerobic conditions. J. Biol. Chem. 281 (38), 27806–27815.

Schaefer, U., Boos, W., Takors, R., Weuster-Botz, D., 1999. Automated sampling device for monitoring intracellular metabolite dynamics. Anal. Biochem. 270 (1), 88–96.

Schaub, J., Reuss, M., 2008. *In vivo* dynamics of glycolysis in *Escherichia coli* shows need for growth-rate dependent metabolome analysis. Biotechnol. Prog. 24 (6), 1402–1407.

Stephanopoulos, G., 1994. Metabolic engineering. Curr. Opin. Biotechnol. 5 (2), 196–200.

Sunya S., Delvigne F., Uribelarrea J.L., Molina-Jouve C., Gorret N. 2012. Comparison of the transient responses of *Escherichia coli* to a glucose pulse of various intensities. Appl. Microbiol. Biotechnol..

Taymaz-Nikerel, H., Borujeni, A.E., Verheijen, P.J.T., Heijnen, J.J., van Gulik, W.M., 2010. Genome-derived minimal metabolic models for *Escherichia coli* MG1655 with estimated *in vivo* respiratory ATP stoichiometry. Biotechnol. Bioeng. 107 (2), 369–381.

Taymaz-Nikerel, H., de Mey, M., Ras, C., ten Pierick, A., Seifar, R.M., van Dam, J.C., Heijnen, J.J., van Gulik, W.M., 2009. Development and application of a differential method for reliable metabolome analysis in *Escherichia coli*. Anal. Biochem. 386 (1), 9–19.

Taymaz-Nikerel, H., van Gulik, W.M., Heijnen, J.J., 2011. *Escherichia coli* responds with a rapid and large change in growth rate upon a shift from glucose-limited to glucose-excess conditions. Metab. Eng. 13 (3), 307–318.

Theobald, U., Mailinger, W., Baltes, M., Reuss, M., Rizzi, M., 1997. *In vivo* analysis of metabolic dynamics in *Saccharomyces cerevisiae*: I. experimental observations. Biotechnol. Bioeng. 55 (2), 305–316.

Trotter, E.W., Rolfe, M.D., Hounslow, A.M., Craven, C.J., Williamson, M.P., Sanguinetti, G., Poole, R.K., Green, J., 2011. Reprogramming of *Escherichia coli* K-12 metabolism during the initial phase of transition from an anaerobic to a micro-aerobic environment. PLoS One 6 (9), e25501.

van Dam, J.C., Eman, M.R., Frank, J., Lange, H.C., van Dedem, G.W.K., Heijnen, S.J., 2002. Analysis of glycolytic intermediates in *Saccharomyces cerevisiae* using anion exchange chromatography and electrospray ionization with tandem mass spectrometric detection. Anal. Chim. Acta 460 (2), 209–218.

Visser, D., van Zuylen, G.A., van Dam, J.C., Oudshoorn, A., Eman, M.R., Ras, C., van Gulik, W.M., Frank, J., van Dedem, G.W., Heijnen, J.J., 2002. Rapid sampling for analysis of *in vivo* kinetics using the BioScope: a system for continuous-pulse experiments. Biotechnol. Bioeng. 79 (6), 674–681.

Wu, L., Mashego, M.R., van Dam, J.C., Proell, A.M., Vinke, J.L., Ras, C., van Winden, W.A., van Gulik, W.M., Heijnen, J.J., 2005. Quantitative analysis of the microbial metabolome by isotope dilution mass spectrometry using uniformly ^{13}C-labeled cell extracts as internal standards. Anal. Biochem. 336 (2), 164–171.

Wu, L., van Dam, J., Schipper, D., Kresnowati, M.T., Proell, A.M., Ras, C., van Winden, W.A., van Gulik, W.M., Heijnen, J.J., 2006. Short-term metabolome dynamics and carbon, electron, and ATP balances in chemostat-grown *Saccharomyces cerevisiae* CEN.PK 113-7D following a glucose pulse. Appl. Environ. Microbiol. 72 (5), 3566–3577.

Yun, H.S., Hong, J., Lim, H.C., 1996. Regulation of ribosome synthesis in *Escherichia coli*: effects of temperature and dilution rate changes. Biotechnol. Bioeng. 52 (5), 615–624.